CHAPTER 6

EVALUATE AEROGELS DERIVED FROM NANOCELLULOSE AND INCORPORATE BIOACTIVE COMPOUNDS FOR USE IN FOOD PACKAGING APPLICATIONS

6.1. Introduction

After harvesting, the stalk to which the banana fingers are attached becomes a major residue of banana cultivation that is discarded into the ecosystem. This residue is called banana rachis and is rich in lignin, hemicellulose, and cellulose fractions. In recent years, researchers have shown interest in using the fibrillar material from rachis in various ways. Zuluaga et al., (2009) suggested that these materials can be useful in reinforcing fillers in nanocomposites. Pelissari et al. (2014) advocated its use as reinforcers of polymer composite systems. Guerrero et al. (2018) found that rachis residues are viable for the production of ethanol under low enzyme dosage and low yeast inoculum.

Chemical treatment is commonly followed to extract cellulose because it is affordable, may remove the lignin and hemicellulose fractions, and can catalyse the breakdown of the fibre cell walls, exposing the cellulose for extraction (Hafid et al., 2021; Ding et al., 2022). In order to create smaller cellulose fibres, the lignin and hemicellulose must first be separated from the cellulose during the extraction process. The cellulose fibres are then acid hydrolysed to eliminate the amorphous parts to obtain crystalline fibre structures (Linan et al., 2021; Bhardwaj et al., 2023; Ospina-Varon et al., 2022).

Biopolymers from agricultural waste can be used to make aerogels, which are three-dimensional nets. They have a porous structure, are solid lightweight materials, and have a low density (Bakhori et al., 2023; Kaur et al., 2023). Numerous investigations have looked into the production of aerogels from natural polymers for usage in food packaging as bioactive component absorbers and carriers (Oliveira et al., 2019; de Oliveira et al., 2019). These aerogels are an environmentally friendly substitute for making food packaging enriched with bioactive compounds that have good water absorption and antioxidant capacity (Fonseca et al., 2021).

Aerogels are substances created by introducing air into the meshes of a gel network to replace the solvent. This replacement occurs throughout the drying process, such as freeze-drying or supercritical drying. Depending on the reaction parameters, aerogels can have a high porosity that is displayed as a mixture of mesopores (2–50 nm), micropores (<2 nm), and macropores (>50 nm), with a remarkable interior surface area. Aerogels are relatively light in weight since they are composed of approximately 95% air or gas by volume (Nita et al., 2020). Aerogels can be made from polyvinyl alcohol (PVA) that forms the matrix using a physical cross-linking process. PVA is a synthetic polymer; thus, it would be ideal if renewable biopolymers like cellulose could replace it, at least in part. Although nanocellulose has outstanding bio- compatibility and biodegradability, aerogels have a tendency to dissolve when in contact with water. Therefore, one alternative to enhance the properties of aerogel is to combine several polymers, including synthetic and natural polymers, to create composite aerogel. This technique abstains from the use of toxic chemical cross-linkers, making it appropriate for food applications.

Aerogels are attractive matrices for the integration and release of bioactive chemicals, because they can be shielded from undesirable outside influences. They preserve bioavailability of compounds, delay their degradation, and enable their regulated and targeted release (Niknia et al., 2020; de Oliveira et al., 2020). The outstanding sorption and desorption capacity of the aerogels confers these desirable properties (Garcia-Gonzalez et al., 2021). The utilization of phenolic compound-rich natural extracts for their antioxidant properties by the food industry has helped to improve shelf stability (Fonseca et al., 2021). Researchers are focussing on creating bioactive- enriched aerogels and searching for their innovative food use. The focus of this research work was to develop aerogel which exhibits high water absorption capacity, show antioxidant activity, and regulate *in-vitro* release of phenolic compounds. The cellulosic aerogels exhibit high porosity that allows for greater loading capacity for bioactive compounds. It is, therefore, expected that the developed aerogels loaded with bioactive substances will show higher antioxidant properties with significant promise for the development of food preservatives and nutraceuticals.

Clitoria ternatea is a plant grown for its aesthetic qualities and is known for its bioactive properties and significant medicinal value. Its edible flower is commonly referred to as blue pea or butterfly pea flower. The high concentration of polyacylated anthocyanins

called ternatins gives blue pea petals their distinct appearance and special characteristics. The use of anthocyanins from blue pea flowers in food aerogels was investigated by Vidana et al. (2021). The flower extract demonstrated excellent antioxidant activity as well as a controlled and regulated *in-vitro* release. Butterfly pea petal extract, however, has not yet been investigated for use in hybrid bioactive aerogels.

Freshness indicators in food packaging often use dyes or pH-sensitive compounds to signal freshness visually. Ghadiri Alamdari et al. (2022) have studied *Ixiolirion tataricum* (Siberian lily), a flower native to Central and Southwest Asia and parts of Northeast Africa, contains phytochemicals like tannins, flavonoids, anthocyanins, organic acids, and flavones, for use as natural colour indicators. These indicators, widely studied in intelligent packaging, typically consist of responsive pigments (e.g., curcumin, anthocyanins) combined with a polymer matrix of co-polymers and fillers (Zheng et al., 2021). Recent research has utilized anthocyanins from food by-products such as purple sweet potato, red cabbage, and blueberry to assess protein-based food freshness (Nabi et al., 2023; Oliveira Filho et al., 2021). In the wine industry, grape pomace—comprising grape skins, seeds, and stalks—contains anthocyanins responsible for the grape's purple colour. These anthocyanins, which shift from pink to blue under different pH conditions, are widely used as intelligent colour indicators (de Souza Mesquita et al., 2023).

The present study focused on the formation and characterization of hybrid aerogels reinforced with PVA, nanocellulose and cellulose isolated from banana rachis, and their incorporation with bioactive compounds extracted from butterfly pea petals. Whether these polysaccharide aerogels are suitable for use as matrices for the release of incorporated bioactive compounds was investigated. Furthermore, the hybrid aerogels that have been produced are employed to track the freshness and spoiling state of minced chicken while it is being stored at 4 °C. To our knowledge, this is the first report on using banana rachis for aerogel development and its application in monitoring the freshness/spoilage of meat products.

6.2. Materials and methods

6.2.1. Materials

Cellulose was extracted from freshly harvested and fully mature banana rachis (*Musa acuminata*, 'Dwarf Cavendish') sourced from local farmers in Tezpur. Chicken was taken

from the local market of Tezpur University, Napaam. Tween-80 (Sigma-Aldrich, purity >99%) along with sunflower oil and standard β-carotene (purity ≥ 93%) were used in the study. Analytical chemicals were sourced from TCI, SRL, and Merck.

6.2.2. RP-HPLC analysis

6.2.2.1. Extraction

Using a probe sonicator (U500, Takashi, Japan), 5 g of lyophilised butterfly pea powder was extracted with 50 mL of methanol: water (60:40, v/v) for 60 min at room temperature (23–25 °C). The mixture was centrifuged for 30 min at 16,000× g (Eppendorf 5430 R, Germany).

6.2.2.2. Purification procedure

The prepared extract (100 µL) was transferred to a centrifuge tube, followed by the addition of 700 µL of ice-cold ethanol. After vortexing for 15 s, the tubes were stored at −80 °C for 60 min. Next, they were centrifuged at 21,000 × g for 30 min. The supernatant was filtered through a 17 mm (0.2 mm) PVDF syringe filter (VWR Scientific, Seattle, WA, USA) and then dried under vacuum at 40 °C. The residue was activated with 6 mL of 100% methanol and passed through a 200 mg C-18 solid-phase extraction cartridge (Waters, MA, USA). It was then washed with 6 mL of water and eluted with another 6 mL of methanol. The methanol fraction, containing the parent anthocyanins, was concentrated to dryness and re-dissolved for HPLC analysis.

6.2.2.3. RP-UHPLC operating parameters

Anthocyanins and their derivatives were analysed using reverse-phase UHPLC (Ultimate 3000, Thermo Scientific, USA) with a DAD detector (1260 Infinity, Agilent, CA, USA). A 3.0 µL injection volume was used, and separations of anthocyanins and anthocyanidin aglycones were performed on a C-18 analytical column (2.1 × 50.0 mm, 1.8 µm, Agilent, CA, USA). The mobile phase consisted of water (solvent A) and acetonitrile (solvent B), each containing 0.1% formic acid. The flow rate was set to 0.3 mL/min, with the following gradient program: 0–5 min, 0–30% B; 5–8 min, 30–75% B; 8–25 min, 75–100% B. UV-Visible absorption spectra for anthocyanins were recorded at 535 nm. The MS conditions were as follows: gas temperature at 275 °C, gas flow at 8 L/min, nebulizer pressure at 45

psi, sheath gas temperature at 350 °C, and sheath gas flow at 12 L/min. The capillary voltage was set to 3500 V (positive and negative), with a nozzle voltage of 500 V (positive and negative). The scan mass range was 270–1000 m/z in positive mode.

The phenolic acids in the extracts were identified following the method of Espin et al. (2016) with some modifications. Freeze-dried samples (5 mg) were extracted with 75% methanol (1 mL) by shaking for 30 minutes, followed by 30 minutes in an ultrasonic bath. After centrifugation at 7000g for 5 minutes, the supernatant was collected. The residue was re-extracted twice, and combined extracts were concentrated, reconstituted in methanol:water (25:75, v/v), sonicated, centrifuged (10,000g, 5 minutes), and quantified using reverse-phase UHPLC (Ultimate 3000, Thermo Scientific, USA) with a C-18 column and diode array detector. The flow rate was set at 0.5 mL/min, the column temperature at 35 °C, and the detection wavelength at 330 nm. The gradient program was as follows: 15% B for 5 min, 20–35% B over 10 min, 35–50% B over 10 min, 50–60% B over 5 min, and 60% B for 5 min.

6.2.3. Development of aerogels using cellulose fibre, nanocellulose, and butterfly pea flower extract

The methodology and formulations used to create the aero- gels are listed in Table 1. Aqueous dispersions of 11% PVA (w/v) and 7% CF (w/v) were blended in the ratio of 3:1 and coded as PVA+CF. Then, PVA+CF+NC was made by replacing 3% (w/w) of the total weight of cellulose with nanocellulose. This composition was based on the most successful outcomes reported by Oliveira et al. (2020). Butterfly pea flower extract (BPFE) was prepared using ethanol aqueous extraction (60%, v/v) in a shaking water bath at 60°C and 100 rpm for 2 hours (1:8 sample-to-solvent ratio). The extract was vacuum-filtered and stored at -20°C (Blue Star, CHFDD300D) until analysis, following Tuan Putra et al. (2021) with modifications. Thereafter, BPFE was added to PVA, PVA+CF, and PVA+CF+NC dispersions to obtain a 3 mg extract/g sample final concentration, and the bioactive aerogels were coded as PVA+BPFE, PVA+CF+BPFE, and PVA+CF+NC+BPFE, respectively. The concentration used was according to Oliveira et al. (2020). The resulting dispersions were kept at 90°C with agitation in a sealed container for 1h. Thereafter, 4 g of the mixture was put into a Petri dish of 5.3 cm diameter. The mixture was subjected to

a physical cross-linking technique that involved five freeze cycles (–20°C) and lastly was freeze-dried.

Table 6.1. Formulations used to develop aerogels and bioactive aerogels.

Sample code	Polyvinyl alcohol (%, w/w)	Cellulose fibre (%, w/w)	Nanocellulose (%, w/w)	Butterfly pea flower extract (%, w/w)
Aerogels (Control)				
PVA	100.0	0.0	0.0	0.0
PVA+CF	82.5	17.5	0.0	0.0
PVA+CF+NC	82.5	17.0	0.5	0.0
Bioactive aerogels				
PVA+BPFE	99.7	0.0	0.0	0.3
PVA+CF+BPFE	82.3	17.4	0.0	0.3
PVA+CF+NC+BPFE	82.3	16.9	0.5	0.3

PVA: Polyvinyl alcohol; CF: Cellulose fibre; NC: Nanocellulose; BPFE: Butterfly pea flower extract

6.2.4. Characterization of developed aerogels

Dynamic light scattering (DLS) technology (Malvern®, Zetasizer Nano ZS, England) was used to determine the size of nanocellulose. The material was dissolved in distilled water at a temperature of 25 °C and ultrasonically processed for 2 min. The size of the nanostructures was quantified in terms of their quantity, intensity, volume, and average size (Hemmati et al., 2018).

The FT-IR-ATR (attenuated total reflectance) spectra were analysed using a spectrometer (Nicolet Instrument 410 FT-IR, Thermo Scientific, USA), and the data was collected at a resolution of 4 cm^{-1} and performed in the spectral region 4000–400 cm^{-1}.

The relative crystallinity was measured using an X-ray diffractometer (D8 FOCUS Bruker AXS, Germany) run at 60 kV with a scanning range of 10 to 80° (2θ). The analysis was

carried out at room temperature at a step size of 0.001°. The X-ray diffractograms were used to calculate the relative crystallinity using **Eq. 6.1** (Rabek et al., 1980):

$$Relative\ crystallinity\ (\%) = \frac{A_c}{(A_c + A_a)} \times 100 \qquad \textbf{Eq. 6.1}$$

where Aa is the amorphous region and Ac is the crystalline region.

Thermogravimetric analyser (TGA) (model # TG 209 F1 Libra, Make # Netzsch, Germany) was used to test the thermal stability of BR, CF, NC, and the aerogels. Samples (6–10 mg) were heated between 30 and 600 °C at a rate of 10 °C min−1. While running the instrument, 20 mL of nitrogen per min was pumped into the system. For calculating the degradation temperature, a derivative thermogravimetric (DTG) curve was produced by plotting the weight change over time (dW/dT) versus temperature (°C).

A field emission scanning electron microscope (JSM-7200F, JEOL, Japan) was used to examine the morphology of the BR, CF, NC, and the aerogels. Immediately after being shattered, the liquid nitrogen-frozen aerogel samples had a thin layer of gold sprayed on them. A 10 kV accelerating voltage was used.

Aerogels' ability to absorb water was assessed using a modified version of the Demitri et al. (2013). The aerogels were dissolved in distilled water (50 mL) in a known quantity at room temperature for 48 h. The water absorption capacity was calculated using **Eq. 6.2**:

$$Water\ Absorption\ Capacity\ (WAC) = \frac{(W_s - W_d)}{W_d} \times 100 \qquad \textbf{6.2}$$

Where, W_d is the weight of the dried sample and W_s is the weight of the swollen aerogels.

The size and weight of each cellulose fibre aerogel were used to calculate the density of the aerogel. **Eq. 6.3** was used to calculate the aerogels' porosity (Geng H, 2018):

$$Porosity\ (\%) = \frac{V - \left[\frac{Wa}{\rho c}\right]}{V} \times 100 \qquad \textbf{Eq. 6.3}$$

Where, W_a is the aerogels' weight in grammes (g), V is their volume (cm^3), and ρc is the density of cellulose (1.528 g/cm^3).

6.2.5. Antioxidant capacity of bioactive aerogels

According to the procedures suggested by Williams et al. (1995) and Oliveira et al. (2020), the ability of the butterfly pea flower extract and aerogels to sequester the radical 1,1-diphenyl-2-picrylhydrazyl (DPPH) served as the basis for evaluating their antioxidant activity. Individual tubes containing samples (1 mg) were weighed, and then 3.9 mL of freshly prepared DPPH solution in methanol was vortexed for 30 s (absorbance adjusted for 1.10±0.02). After 2 h and 30 min, the absorbance at 515 nm was measured, and **Eq. 6.4** was used to calculate the capacity to sequester the radical in percentage in comparison to the control:

$$\%inhibition = \frac{ABS_{control} - ABS_{sample}}{ABS_{control}} \times 100\% \qquad \textbf{Eq. 6.4}$$

6.2.6. In-vitro release of bioactive aerogels from cellulose fibre and nanocellulose

In accordance with the European Commission Regulation (10/2011/EU), 50% ethanol and 10% ethanol are each regarded as food simulants for hydrophobic and hydrophilic food products, respectively, and were used in the *in-vitro* release assays of the bioactive aerogels. The technique utilized to create the release profiles was obtained from Oliveira et al. (2019) and Oliveira et al. (2020). In brief, at normal room temperature, 2 mL of the food simulant solution was soaked in 160 mg of aerogel samples. Using supernatant's absorbance at 301 nm, wavelength was measured at appropriate time intervals in a spectrophotometer (Cary 60 UV-Vis, Agilent) to evaluate the concentration of bioactive BPFE in the release medium (Costamagna et al., 2017). The complete spectrum of BPFE dissolved in 10% and 50% ethanol was previously recorded with varying concentrations from 0.4 to 4 (mg/ mL) in order to establish a calibration curve. The amount of bioactive BPFE that was released from the aerogels at each interval was determined from the collected data. Each sample was examined in three independent replicates.

6.5.7. Colour stability, reversibility, and colour change of bioactive aerogels under different pH conditions

To assess colour stability, the chosen bioactive aerogels (2 cm × 2 cm) were stored for 30 days under three conditions: at 4 °C in darkness, and at 20 °C in both dark and light conditions. To examine the colour reversibility of the bioactive aerogels, samples (3 cm ×

3 cm) were exposed to 50 mL of ammonia vapor (0.8 mol/L) for 3 min, followed by exposure to 50 mL of acetic acid vapor (99.7%) for 3 min. This test was conducted over three cycles, and images of the indicators were recorded. To evaluate colour changes in bioactive aerogels under different pH levels, 2 cm × 2 cm sections of the aerogels were immersed in solutions with pH values ranging from 2 to 13 for 5 min. Colour transformations at each pH level were documented using a digital camera (Mirmoeini et al., 2023).

6.2.8. Application of developed aerogels in the detection of minced chicken spoilage

To monitor spoilage in minced meat, 30 g of minced meat was placed in a polyethylene terephthalate (PET) box, with an aerogel sample (1 × 1 × 0.5 cm) positioned on a sterile Petri plate inside the package, avoiding direct contact with the meat. The packages were sealed and stored at 4 °C for 9 days. Chemical and microbial analyses, along with ΔE colour measurements of the aerogel, were conducted in triplicate on days 0, 3, 6, and 9.

6.2.8.1. pH measurement

To measure pH, 10 g of the meat sample was homogenized in 90 mL of distilled water, and pH was measured by a digital pH meter (Mettler Toledo, UK).

6.2.8.2. Total volatile bases-nitrogen (TVB-N) content

The TVB-N was measured following the method of Mirmoeini et al. (2023). For this,10 g of the sample was homogenized in 300 mL of distilled water, filtered, and transferred to a flask. Then, 2 g of MgO was added, and the mixture was heated to boiling. After a 25-min distillation of the volatile nitrogen base, the distillate was collected in an Erlenmeyer flask containing 2% boric acid and a bromocresol green/methyl red indicator. The solution was then titrated with 0.1 N sulfuric acid until a red colour appeared. TVB-N was calculated based on mg of nitrogen/100 g of meat (**Eq.6.5**).

$$\text{TVB} - \text{N contents } \left(\frac{\text{mg}}{100\ \text{g}}\right) = (V_1 - V_0) \times 14 \qquad \textbf{Eq. 6.5}$$

In **Eq. 1**, V_1 and V_0 represent the volumes of sulfuric acid used to titrate the meat samples and the blank distilled water, respectively.

6.2.8.3. Microbial analysis

To quantify mesophilic bacteria, 10 g of meat sample was homogenized in 90 mL of 0.1% peptone water and serially diluted. Appropriate dilutions were then plated on plate count agar and incubated at 37 °C for 48 h. The mesophilic bacterial population was expressed as $\log_{10}$ CFU/g.

6.2.9. Statistical analysis

For the assessment of antioxidant activity, porosity, and density, analytical determinations were made in three separate batches. Tukey test was used to compare the means at a significance level of 5%.

6.3. Results and discussion

6.3.1. HPLC of anthocyanins present in butterfly pea flower

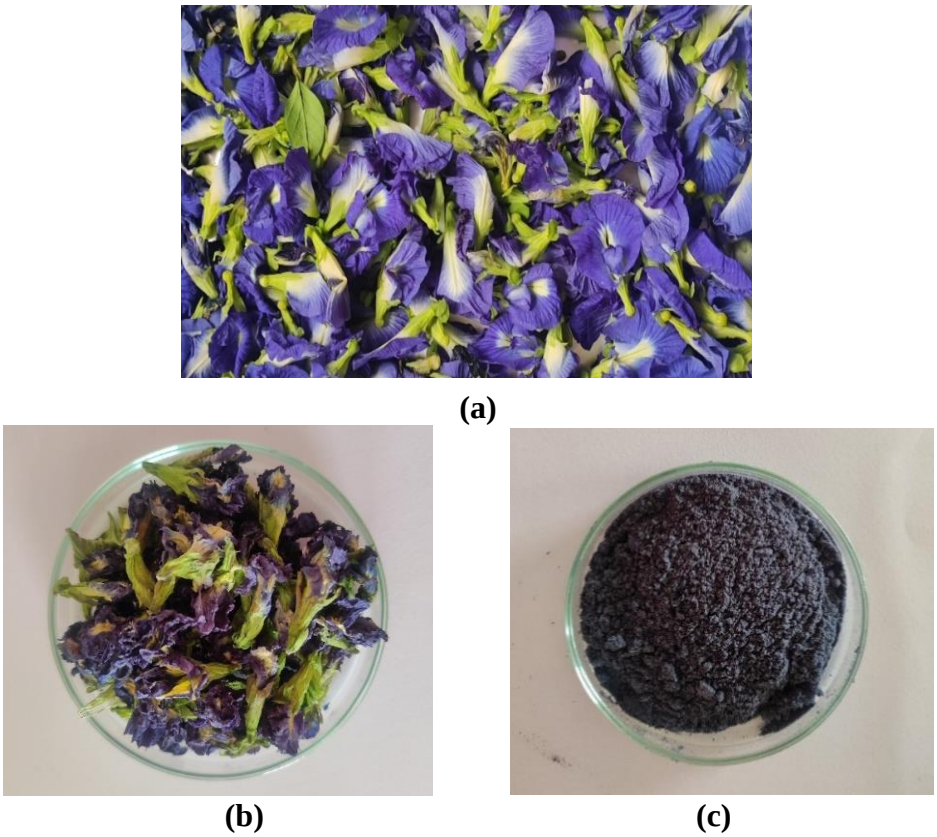

Fig. 6.1. Image of the (a) raw butterfly pea flower (b) Freeze dried, and (c) Powder form of flower.

The identification of anthocyanins peaks in butterfly pea flower extract was primarily based on retention times observed in chromatograms at a 330 nm detection wavelength. The images of the fresh raw butterfly pea flower, freeze-dried, and powdered form are shown in **Fig. 6.1**. Three key anthocyanins were detected: delphinidin derivatives, cyanidin derivatives, and pelargonidin derivatives, each contributing distinct characteristics to the flower's pigmentation. Delphinidin and cyanidin derivatives are primarily responsible for the characteristic blue hue of butterfly pea flowers, whereas pelargonidin, though less abundant, may contribute additional colour nuances.

In the chromatogram presented in **Fig. 6.2**, peak 1 is attributed to delphinidin-3-rutinoside, a compound that contributes significantly to the flower's vivid blue colour. Peak 2 represents cyanidin-3-rutinoside, another vital pigment enhancer, while peak 3 corresponds to pelargonidin-3-rutinoside, which adds a subtle variation in the colour spectrum (Ultraviolet et al., 2021). These identifications provide valuable insights into the anthocyanins composition of butterfly pea flower and support further exploration of their potential applications in food and natural dye industries.

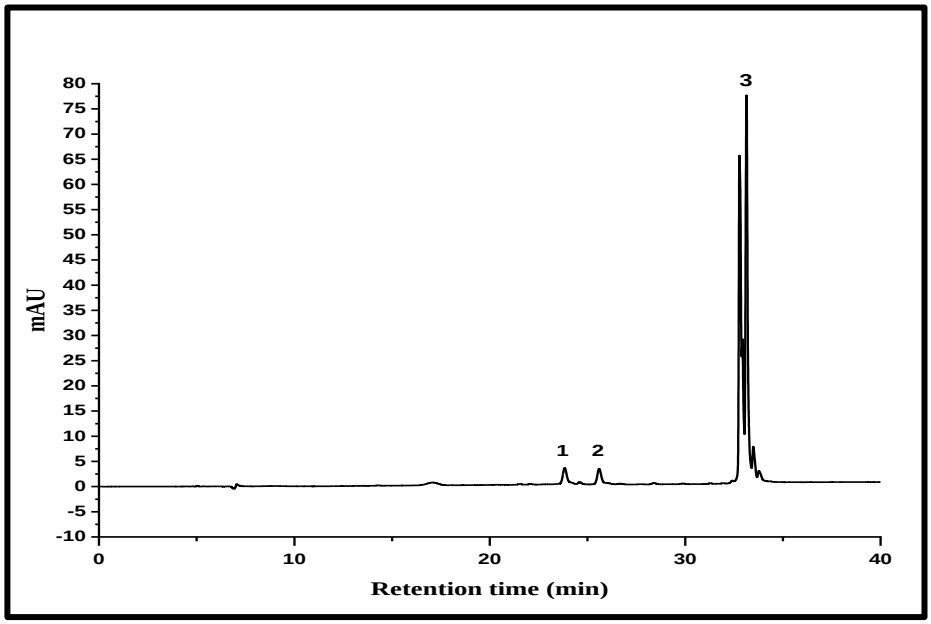

Fig. 6.2. Chromatogram of the butterfly pea flower extract detected at 330 nm. Peak 1, Delphinidin-3-rutinoside; peak 2, Cynadin-3-rutinoside; and peak 3, Pelargonidin-3-rutinoside.

6.3.2. HPLC of phenolic acids present in butterfly pea flower

The phenolic acids profile of butterfly pea flower extract was characterized through HPLC analysis, with detection at 330 nm. Four distinct phenolic acids were identified in the samples, as illustrated in **Fig. 6.3**. These identified compounds include gallic acid, chlorogenic acid, caffeic acid, and p-coumaric acid, each known for its antioxidant and health-promoting properties.

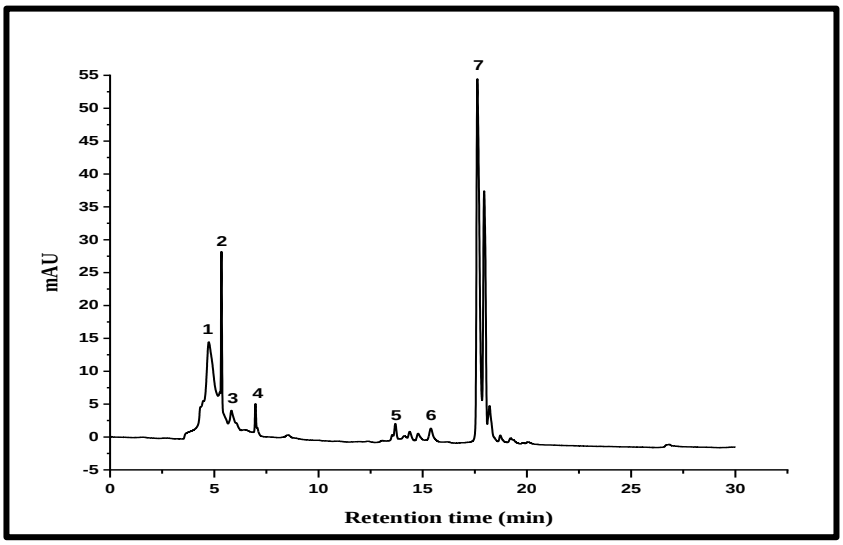

Fig. 6.3. Chromatogram of the butterfly pea flower extract detected at 330 nm. Peak no. 1,2,3, not yet identified; 4: Gallic acid; 5: Chlorogenic acid; 6: Caffeic acid; 7: *p*-Coumaric acid.

The chromatogram displayed several peaks, with peak 4 corresponding to gallic acid, a potent antioxidant known for its free radical-scavenging abilities. Peak 5 indicated the presence of chlorogenic acid, which is widely studied for its role in metabolic health. Peak 6 identified caffeic acid, another phenolic compound with anti-inflammatory and antioxidant benefits, while peak 7 denoted p-coumaric acid, which is known for its antimicrobial properties (Wong & Tan, 2020). Peaks 1, 2, and 3 remain unidentified, suggesting potential minor components or novel compounds. This profiling enhances the understanding of the phenolic composition and potential applications of butterfly pea flower extract in nutraceuticals and functional foods.

6.3.3. Characterization of bioactive aerogels

Figure 6.4 displays the images of the aerogels prepared with PVA, PVA/CF, PVA/CF/NC, PVA/BPFE, PVA/CF/BPFE and PVA/CF/NC/BPFE. The butterfly pea flower had a total phenolic content of 26.4 ± 0.14 mg gallic acid equivalents per g of dry weight, indicating its rich antioxidant potential. To develop bioactive-rich aerogels, the flower extract was incorporated according to the formulations outlined in **Table 6.1**.

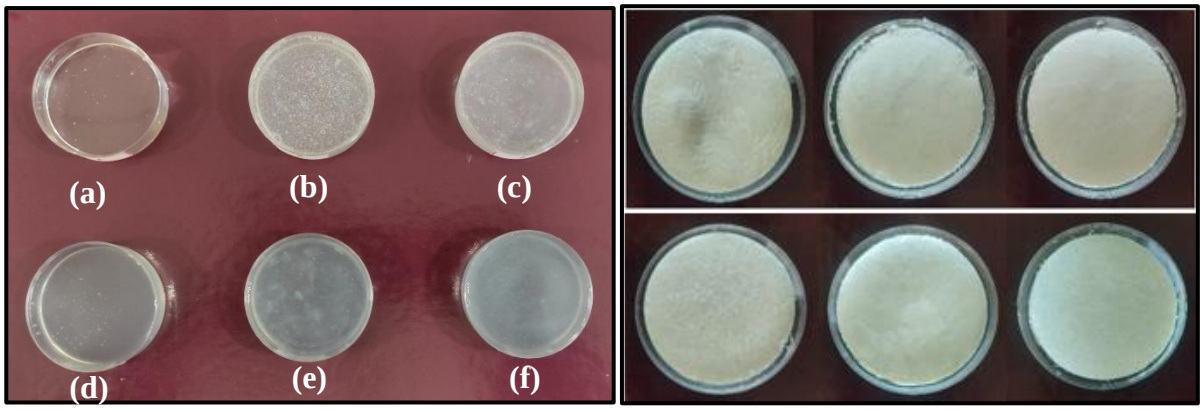

Fig. 6.4. Image of aerogels prepared with (a) PVA, (b) PVA/CF, (c) PVA/CF/NC, (d) PVA/BPFE, (e) PVA/CF/BPFE, and (f) PVA/CF/NC/BPFE before freeze drying.

6.3.3.1. Morphology of the aerogels

The morphology of PVA, PVA+CF, PVA+CF+NC, PVA+BPFE, PVA+CF+BPFE, and PVA+CF+NC+BPFE aerogels was examined using field emission scanning electron microscopy (FE-SEM) and the images are presented in **Fig. 6.5**. Without any polymer phase separation, all the formulations produced homogeneous aerogel structures. Cellulosic materials were seen entangled in polymer matrices (**Fig. 6.5a–f**).

The aerogel that was created using pure PVA had a less porous and more compact structure (**Fig. 6.5a**). The aerogels created with PVA+CF and PVA+CF+NC, on the other hand, in addition to porosity, revealed a three-dimensional, interlinked network structure. The three-dimensional network of the aerogels with CF and NC, however, was more organized than that of the other aerogels (**Fig. 6.5a and b**). Esquivel-Castro et al. (2019) claimed that the structure of a cellulosic aerogel is typically a randomly distributed porous network, with the orientation of the pores depending on the mixture of the raw materials. The morphology of the aerogels after the addition of BPFE did not show any major changes in the internal structure (**Fig. 6.5d–f**).

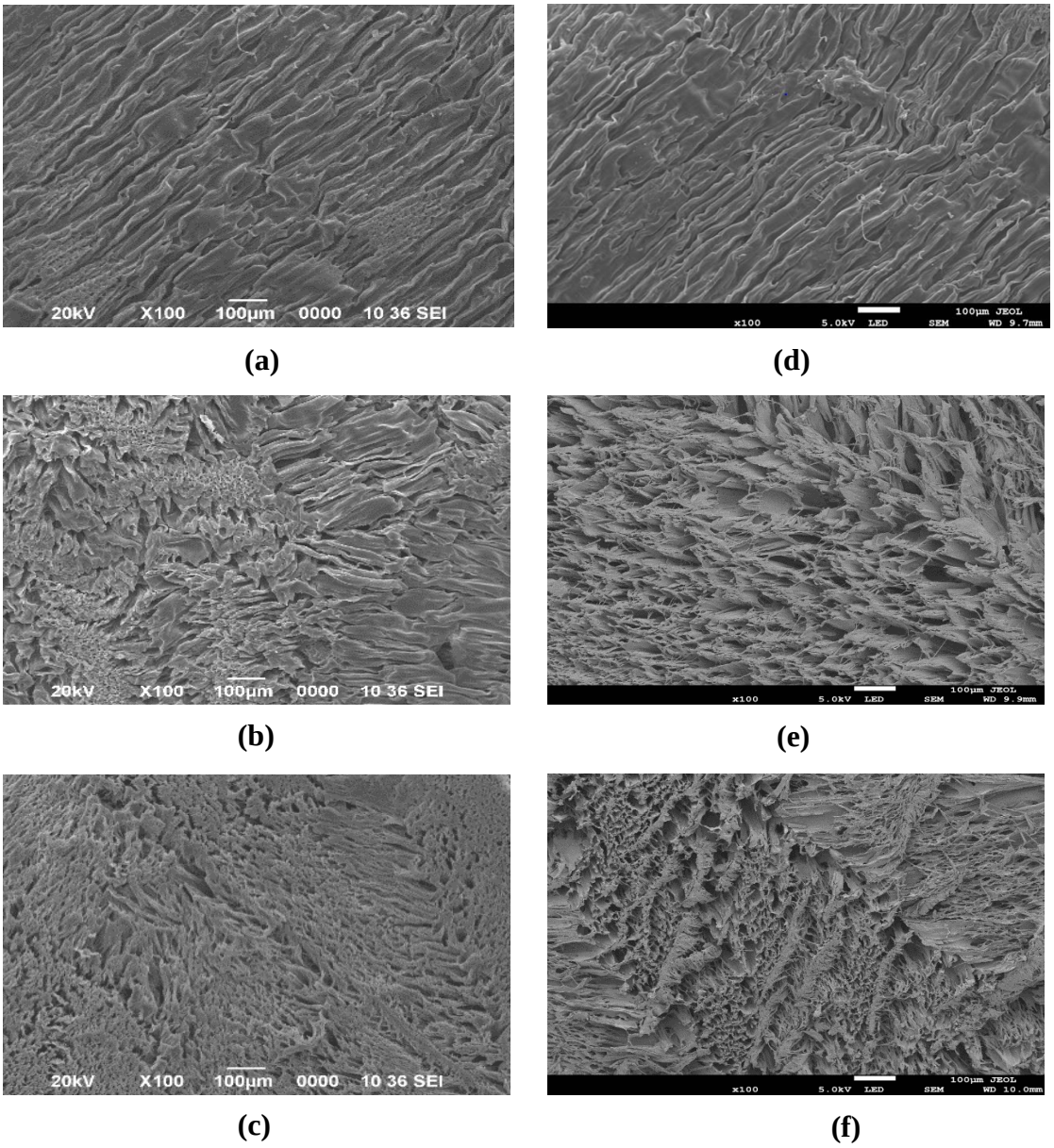

Fig. 6.5. Morphology of aerogels made with (a) PVA, (b) PVA+CF, (c) PVA+CF+NC, (d) PVA+BPFE, (e) PVA+CF+BPFE, and (f) PVA+CF+NC+BPFE. PVA: polyvinyl alcohol; CF: cellulose fibre; NC: nanocellulose; BPFE: Butterfly pea flower extract.

According to researchers, incorporating NC in an aerogel matrix may enhance its ability to absorb water because aerogels with tiny, interconnected pores form favourable pathways that let water move through the matrix by capillary action. In addition, increasing the number of hydrophilic groups in the aerogel matrix by adding NC makes it easier for liquids to diffuse into the matrix (de Oliveira et al., 2019; Abraham et al., 2013).

6.3.3.2. FT-IR spectroscopic analysis

There were recognizable bands in the spectra of the pure PVA aerogels (**Fig. 6.6**), including a broad band with a centre at about 3300 cm^{-1}, which is attributed to O–H stretching from inter- molecular and intramolecular hydrogen bonding. Peaks at 1730 cm^{-1} are attributed to the C=O stretching from residual acetate (Sukudom et al., 2019), whereas bands between 2840 and 3000 cm^{-1} are caused by the C–H stretching from alkyl groups (Peresin et al., 2010; Jayasekara et al., 2004). It was difficult to tell which bands formed as a result of the cellulose's integration into the hybrid aerogels because the most recognizable cellulose bands merged with the PVA matrix bands. However, when cellulosic components were introduced into the aerogels, the bands between 3600 and 2800 cm^{-1} underwent a considerable structural alteration (de Oliveira et al., 2019). Olivera et al. (2020) suggested that there are fewer hydrophilic interactions between cellulose and PVA as a result of the band around 2900 cm^{-1} that is observed in neat PVA temporarily switching to a lower wavelength (approximately 2885 cm^{-1}) in the aerogels.

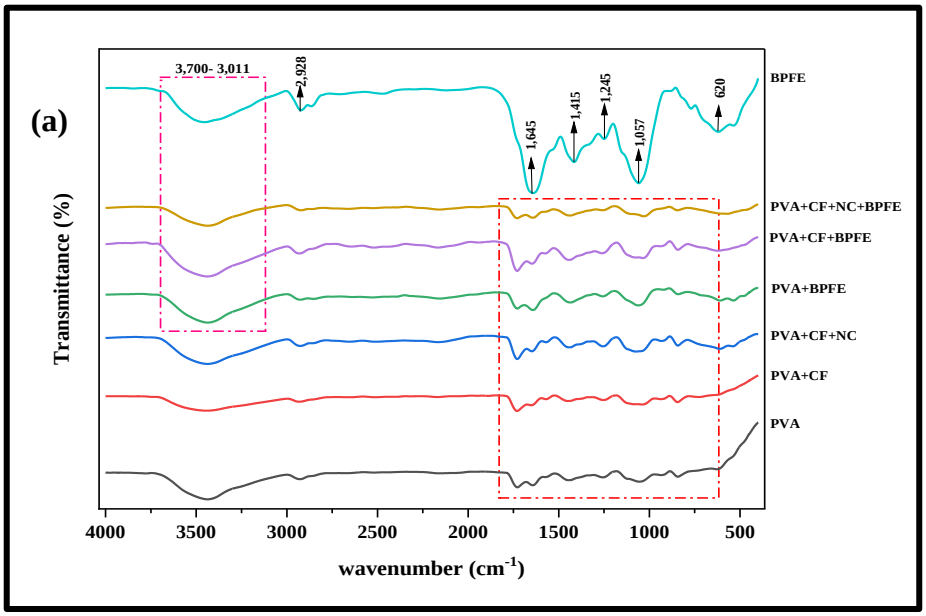

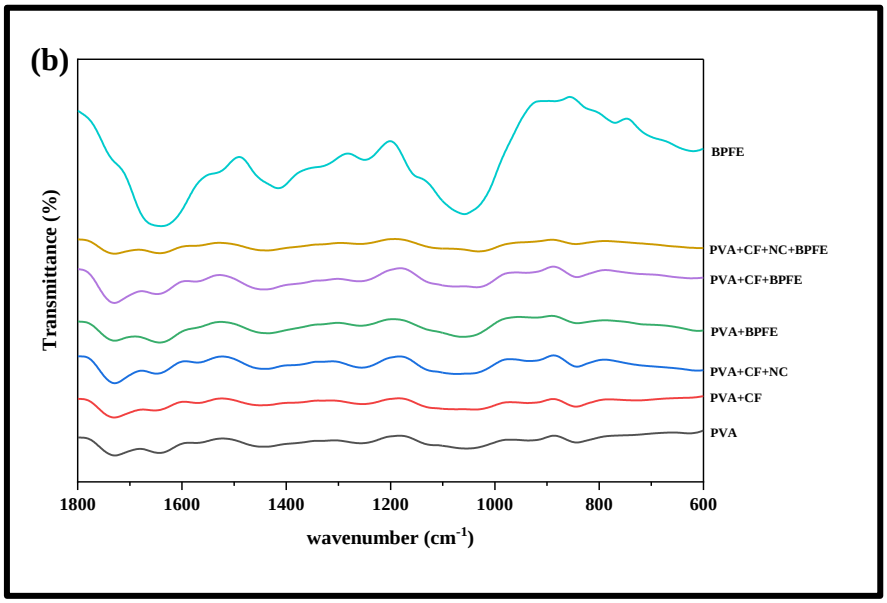

Fig. 6.6. (a) FT-IR spectra of the bioactive and non-bioactive aerogels, (b) expansion of the zone between 1800 cm^{-1} and 600 cm^{-1}.

The FT-IR spectra of aerogels without the addition of BPFE showed the characteristic patterns of cellulosic substrates, with strong bands at around 2900 cm^{-1} and 1027 cm^{-1}, associated to the vibration of the C–O–C and C–H groups of glucose units, respectively. The stretching vibration of the hydroxyl group on the CH_2–OH and CH–OH of the cellulose molecule was linked to a maximal absorption zone at 3440 cm^{-1}, which was observed in the 3700 to 3000 cm^{-1} range.

The BPFE interaction in the aerogel matrix was investigated using FT-IR analysis (**Fig. 6.6a**). The BPFE spectra revealed a broad zone between 3700 and 3100 cm^{-1} (shown in red) that is also present at a comparable intensity in the bioactive-rich aerogels (such as the BPFE-treated aerogels). But in case of aerogel with no BPFE, the intensity of the peak increases. The presence of phenols and alcohols, which correspond to the hydroxyl and O–H stretching frequencies, is confirmed by this band. The region in 1800–500 cm^{-1}, which was identified in BPFE and in the spectra of the bioactive aerogels in a similar way, corresponds to the fingerprint of BPFE (**Fig. 6.6b**). The existence of some alkane compounds is indicated by the peak at 2928 cm^{-1} that is caused by the C–H stretching and found in BPFE and bioactive aerogel. The band at 1645 cm^{-1} indicates that carboxylic

acids are present. Alkyl halides, aliphatic amines, and aromatics are all confirmed by the peak values at 1415 cm^{-1}, 1247 cm^{-1},
and 1063 cm^{-1}, respectively. The similarities between the bioactive aerogels and the BPFE bands indicate that BPFE has been incorporated into the matrix of the aerogels.

6.3.3.3. XRD analysis

Figure 6.7 shows that the peak intensities of PVA and BPFE were milder than those incorporated with CF and NC. The high RC of aerogels seen in **Table 6.2** was the result of the addition of CF and NC. PVA, being an artificial hydrophilic polymer, forms crystallites on repeated freezing and thawing cycles. de Oliveira et al. (2019) have observed that the features of PVA, such as its mechanical strength, water barrier capability, and thermal stability, can be enhanced with the addition of nanomaterials.

Table 6.2. Relative crystallinity and 2θ values of control and bioactive aerogels.

Aerogels	Relative Crystallinity (%)	2θ (°)
BPFE	44.58	21.27, 41.54
PVA	48.37	18.48, 41.34
PVA+BPFE	47.04	18.78, 41.44
PVA+CF	65.27	18.48, 31.36, 41.14
PVA+CF+BPFE	64.21	19.18, 31.65, 41.64
PVA+CF+NC	68.98	19.48, 30.96, 41.24
PVA+CF+NC+BPFE	66.53	19.28, 40.74, 56.01

PVA: Polyvinyl alcohol; CF: Cellulose fibre; NC: Nanocellulose; BPFE: Butterfly pea flower extract

Aerogel of PVA+CF+NC showed higher RC values than PVA+CF+NC+BPFE, which could be explained by the BPFE's relatively low crystallinity (44.58%). The three fillers (CF, NC, and BPFE) in these formulations may also have prevented the PVA matrix from crystallizing, which may have contributed to the decline in the crystallinity of bioactive aerogels.

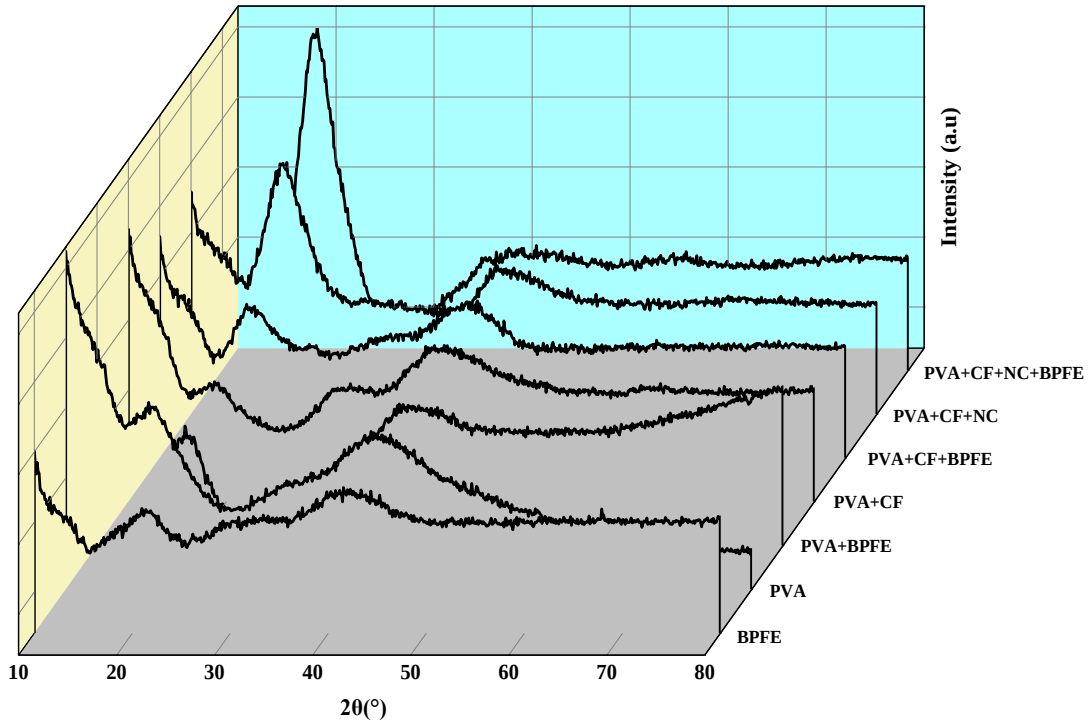

Fig. 6.7. Overlaid powdered XRD pattern of aerogels with and without BPFE. BPFE: butterfly pea flower extract.

6.3.3.4. Thermogravimetric analysis (TGA)

Figure 6.8 shows the thermogravimetric analysis of the aerogels. Thermal decomposition temperatures were also calculated using the first derivative curve (DTG) presented in **Fig. 6.8b**. According to Mary et al. (2020), the first area of thermal deterioration in the BPFE thermogram was observed around 150°C and was caused by the breakdown of the low molecular weight BPFE components. Compounds having more complex properties are considered to degrade in the second zone, which is around 340°C (Mary et al., 2020).

Aerogels made of CF or CF/NC with or without BPFE were discovered to have thermal degradation peaks that were similar to those of the corresponding raw materials, although generally, the thermal deterioration around 320°C is related to the pyrolysis of the CF composition (Ramiah, 1970).

The thermal breakdown temperatures of the bioactive aerogels with BPFE were lower when compared to aerogels without it. This reduction in the thermal degradation

temperature (**Fig. 6b**) may be attributed to the nature of BPFE, which includes substances like phenolic compounds, which are thermally unstable (Wong & Tan, 2020). Given that the BPFE, when investigated alone, begins to disintegrate at about 100°C, it is still reasonable to hypothesize that the aerogels' matrix protects against thermal degradation at temperatures below 200°C.

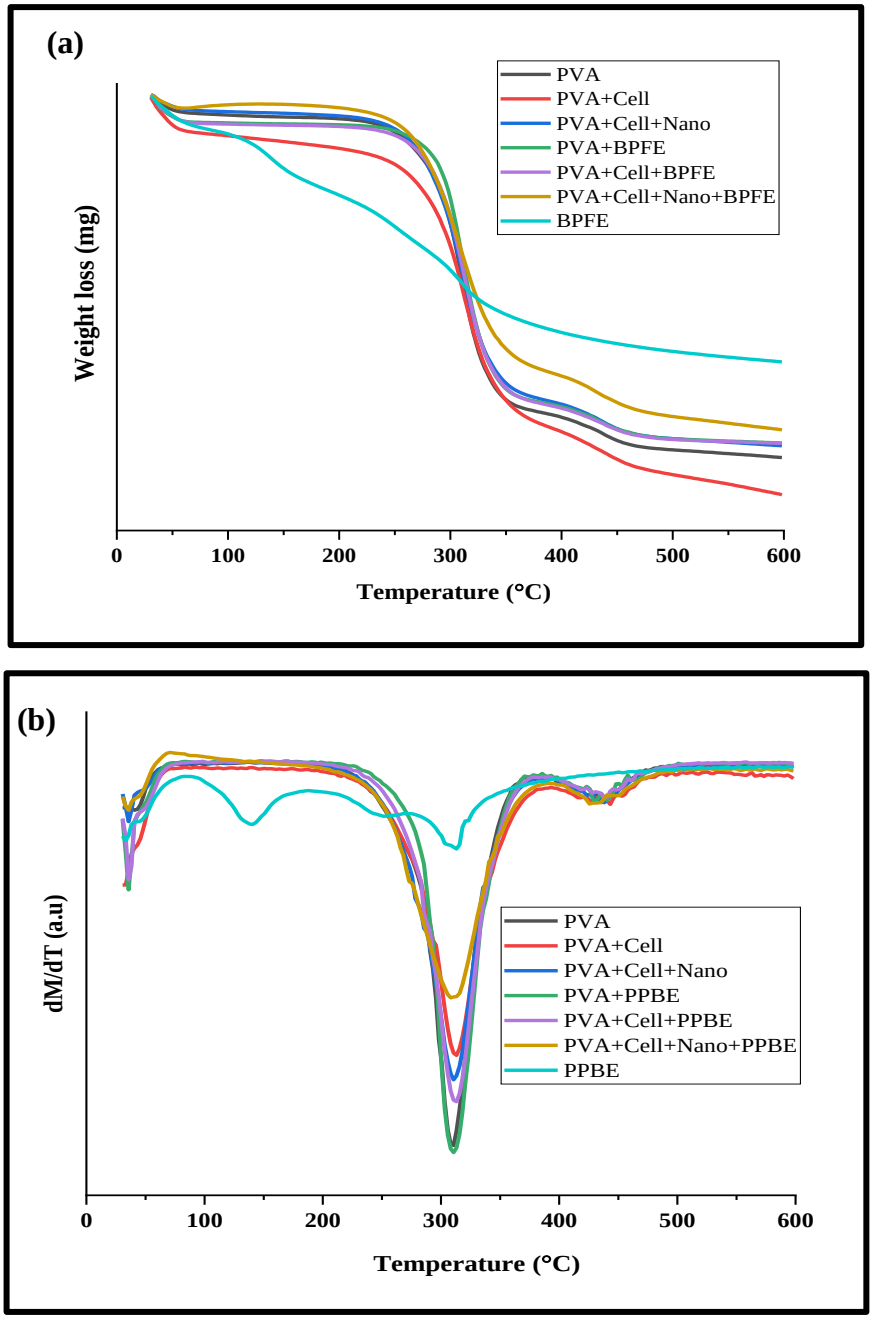

Fig. 6.8. (a) Thermal analysis (TGA), and (b) its first derivatives (DTG) of the aerogels with and without BPFE. BPFE: butterfly pea flower extract.

6.3.3.5. Density, porosity, and water absorption capacity

The addition of cellulosic components significantly reduced the aerogel's porosity ($p<0.05$), as shown by its density and porosity (**Table 6.3**). Other studies have demonstrated that the hybrid aerogel matrix's density values were reduced when CF and NC were added (Fontes-Candia et al., 2019).

Table 6.3. Density and porosity of control and bioactive aerogels.

Sample code	Density ($g.cm^{-3}$)	Porosity (%)
PVA	0.10 ± 0.00^{a}	93.18 ± 0.09^{c}
PVA + CF	0.09 ± 0.00^{b}	94.02 ± 0.09^{b}
PVA + CF + NC	0.07 ± 0.00^{c}	95.21 ± 0.09^{a}

PVA: Polyvinyl alcohol; CF: Cellulose fibre; NC: Nanocellulose; BPFE: Butterfly pea flower extract. For each parameter, values with different letter values in the same column indicate a significant difference according to the Turkey's test ($p<0.05$).

Porosity had an influence on the aerogel structure; as seen in **Fig. 6.5a–c**, more open structures were seen as porosity increased (**Table 6.3**), which also affected the way water absorbed into the material (**Fig. 6.9**). The extremely porous nature of these materials offers substantial advantages while producing superabsorbent materials or using cellulose aerogels as a matrix for the release of bioactive components (Fontes-Candia et al., 2019).

Aerogels manufactured with CF and CF+NC had water absorption capabilities of 1116.99% and 1821.66%, respectively, whereas aerogels made with pure PVA had the lowest water absorption capacity at 460.66% (**Fig. 6.9**). **Table 6.3** demonstrates that aerogels developed with CF and CF+NC have low densities and a high surface area, both of which contribute to their high capacity for absorption (Mi et al., 2018).

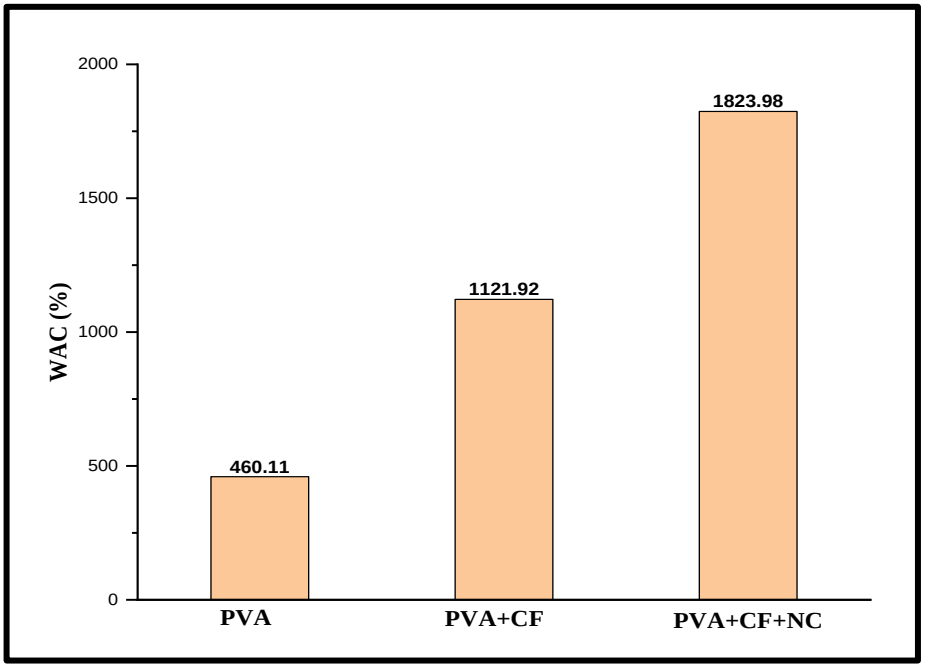

Fig. 6.9. Water absorption by aerogels made of PVA, PVA+CF, and PVA+CF+NC.

The significant levels of water absorption were already anticipated due to the hydrophilic nature of the components used to construct aerogels. CF and CF+NC-based aerogels have a higher capacity to absorb water due to the bigger surface area and increased porosity of cellulosic aerogels; this results in a greater capacity for absorption and a loading capacity for bioactive compounds (Peresin et al., 2010). The observations made through the SEM images (**Fig. 6.5a–f**) further confirm that aerogels containing CF+NC have larger number of open pore microstructure networks that can store more water. Because the hydrophilicity has somewhat increased, they might be able to maintain their integrity for a prolonged period, which might allow water to soak via the capillaries (Madyan et al., 2019). The reason for the pure PVA aerogels' reduced ability to absorb water may be due to their weak network structures that collapsed on contact with water (**Fig. 6.9**).

6.3.3.6. Antioxidant activity of the bioactive aerogels

An evaluation of antioxidant activity was done to confirm the bioactivity of the aerogels (**Fig. 6.10**). Despite the fact that the bioactive aerogels' antioxidant activity was lower (70%) ($p<0.05$) than that of pure BPFE (75%), the freeze-drying and physical cross-linking processes that were used to create the aerogels were unable to reduce the extracts' antioxidant capacity. The addition of NC in aerogels along with CF has further resulted in

a decrease in the antioxidant activity of aerogels; this may be because of the addition of one more filler, i.e. NC in the aerogel matrix, which reduced the availability of BPFE for interaction with DPPH (Zhong et al., 2015; Pang et al., 2019). A variety of food products use the butterfly pea flower as a natural source of blue colourant because of the anthocyanins that are abundant in the petals. Its potential applications in modern health, agriculture, and as a source of natural colouring pigments and antioxidants for food stuff applications have made it very attractive (Zhong et al., 2015; Mehmood et al., 2019).

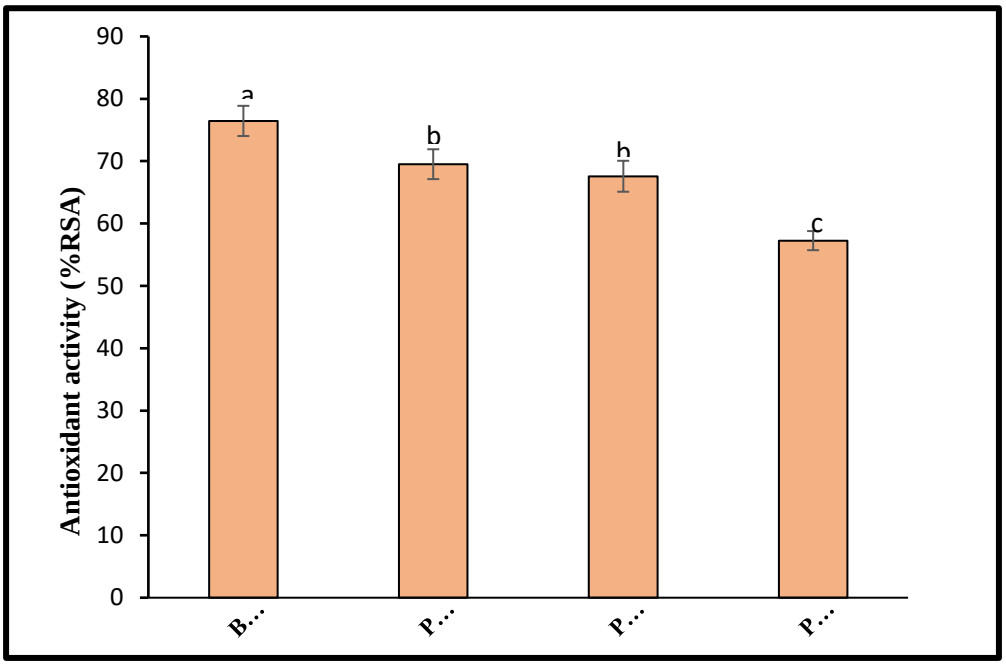

Fig. 6.10. BPFE's and a bioactive aerogels' antioxidant properties. The data here at are presented as the mean (n=3), and the standard deviation is shown by the bars in the columns. Significant differences between values in a column for each letter ($p<0.05$).

The *C. ternatea* flower has higher antioxidant properties than those of other medicinal plants because it contains the anthocyanins (Jeyaraj et al., 2021). We can therefore, draw the conclusion that BPFE injected into polymeric matrices, such as cellulosic aerogels, has significant promise for the development of food preservatives and nutraceuticals.

6.3.3.7. In-vitro release of butterfly pea flower extract from bioactive aerogels

The BPFE release profile was evaluated under the conditions that mimicked hydrophilic foods (10% ethanol) and hydrophobic foods (50% ethanol) as illustrated in **Fig. 6.11a and b**, respectively. BPFE was gradually and slowly released from the CF and CF+NC

aerogels' matrix in both mediums. The medium containing 10% and 50% ethanol caused the aerogels made from neat PVA to lose their structural integrity, which facilitated the bioactive compound's quick release.

The aerogels containing CF+NC demonstrated enhanced and uniform release properties in the hydrophilic food simulant medium (ethanol 10%, **Fig. 6.11a**), as well as preserved their structural integrity for more than 50 h while gradually releasing the BPFE from their matrix. According to Dai et al. (2018), the collapsing of the structure in aqueous solution as a result of the tension formed within the pores is the main cause of the high rate of chemical release from aerogels with hydrophilic properties. Moreover, the aerogel's higher hydrophilicity and lower density can significantly alter the free volume percentage, influencing the release kinetics (Pang et al., 2019).

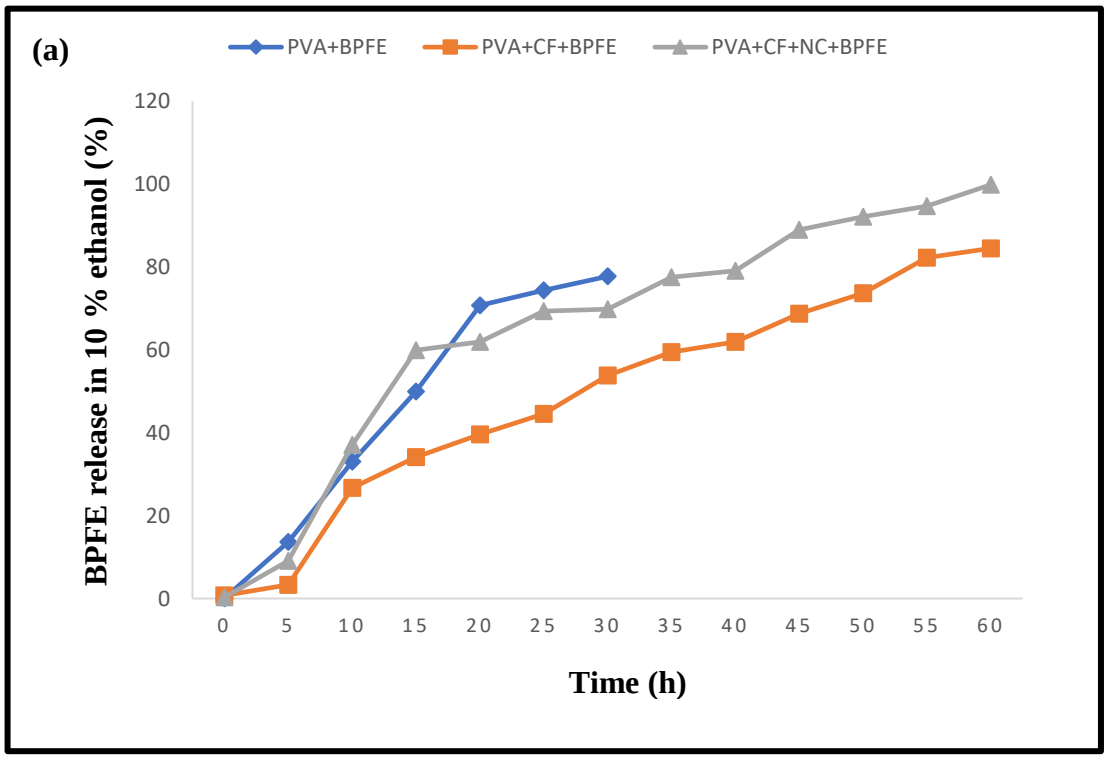

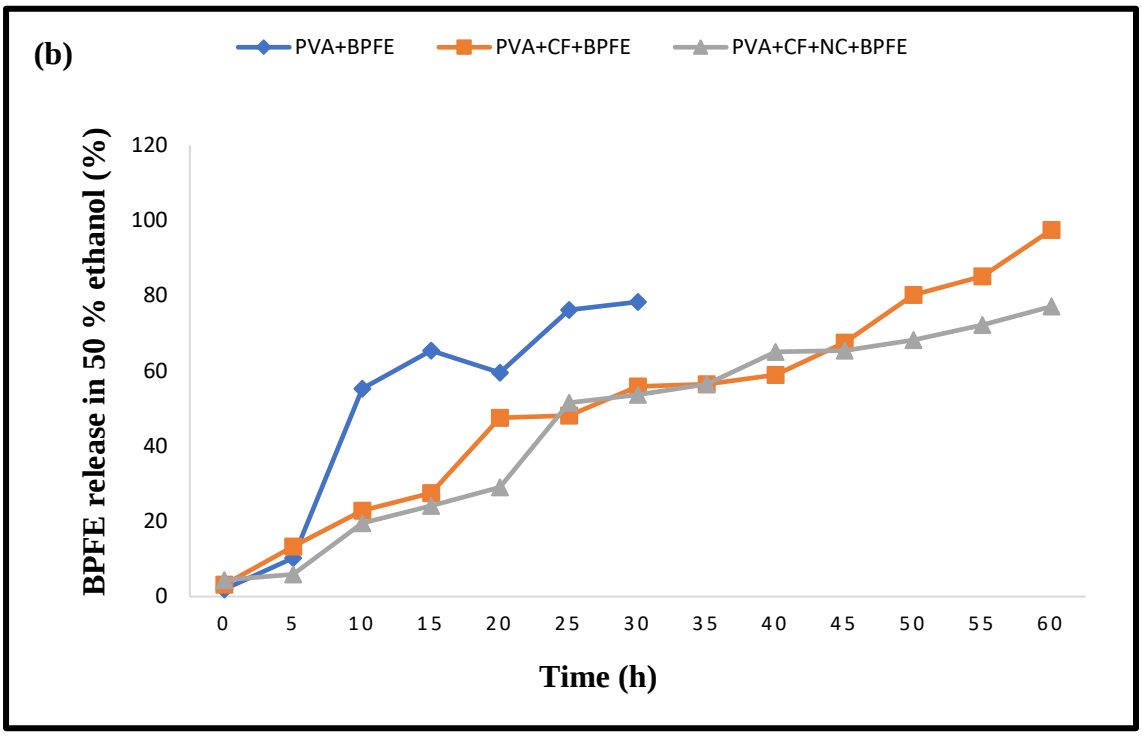

Fig. 6.11. In-vitro release of BPFE from aerogels under (a) hydrophilic and (b) hydrophobic food simulation conditions.

However, in the hydrophobic food simulant media (ethanol 50%, **Fig. 6.11b**), the aerogel containing CF showed improved release kinetics. This process might have occurred because of the polymeric cellulose chain, as suggested by Oliveira et al. [17]. The hydrophilic property of the cellulose chain is balanced by the hydrophobic nature of the pyranose rings. As a result, the cellulose molecules' interactions become anisotropic, which causes a complex conflict between its hydrophilic and hydrophobic properties (Malaspina & Faraudo, 2019). Because of this, the CF-based aerogel and hydrophobic food-simulating media interacted more strongly, allowing the hydrophobic medium to be incorporated and the BPFE to be released simultaneously. Particularly when compared to net PVA aerogels, it is interesting to note that the aerogel treated with CF+NC showed delayed and slow release while demonstrating distinct release kinetics in the two food simulant conditions. As a result, CF+NC-based aerogels showed potential for use as BPFE delivery systems in food packaging.

6.3.3.8. Sensitivity, reversibility, and stability of colour change in bioactive aerogel

The colour response of bioactive aerogels at various pH levels (Fig. 6.12) was analysed to identify their optimal application. The most distinct colour changes, after exposure to acidic and alkaline vapours, were observed with an anthocyanin concentration of 0.44 mg/100 ml. Anthocyanins in the bioactive aerogels act as pH-sensitive colour indicators, transitioning from purple to dark green across a pH range of 3 to 10 with different buffer solutions. Typically, colour alterations in freshness indicators occur following the chemical breakdown of proteins and the release of volatile bases.

A critical finding from the colour reversibility test (Fig. 6.13) was that the aerogels did not revert to their original colour after undergoing repeated cycles of exposure to acidic and basic vapours. This irreversibility aligns with an essential characteristic of freshness indicators, as noted by Abedi-Firoozjah et al. (2023). Reversible colour changes could lead to inaccurate freshness assessments if packaging damage or gas leakage occurred, creating misleading signals for consumers.

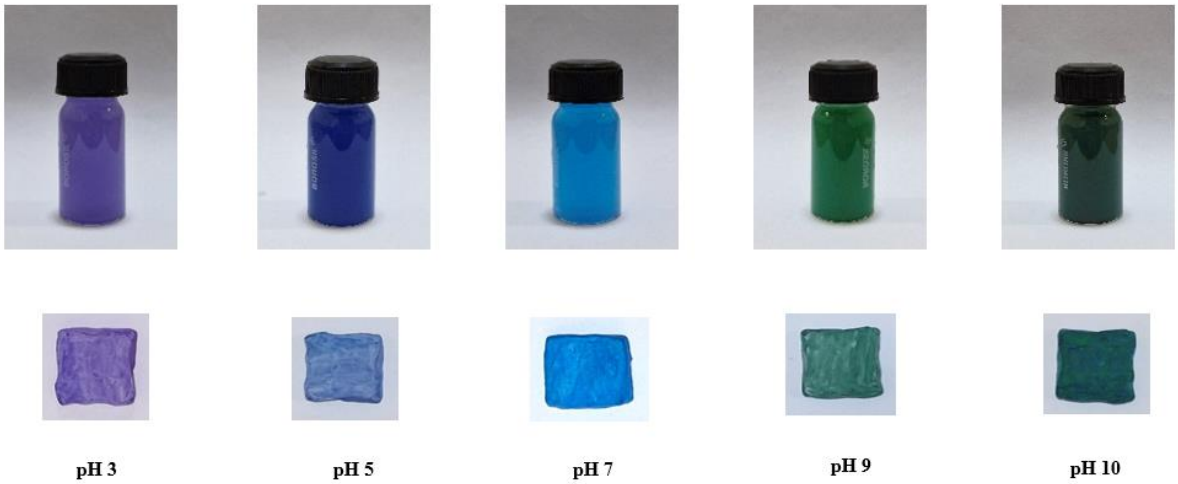

Fig. 6.12. Colour change response of butterfly pea flower (BPF) solution and BPF based aerogels at pH 3, 5, 7, 9 and 10.

The initial light purple hue of the aerogels shifted to dark green due to electron delocalization of anthocyanins when exposed to high hydroxyl concentrations at elevated pH levels (Ghorbani et al., 2022). This irreversible colour change enhances the reliability of bioactive aerogels in smart packaging, effectively preventing food fraud and ensuring accurate spoilage detection.

Figure 6.13 illustrates the colour response reversibility of bioactive aerogels subjected to repeated exposures to ammonia and acetic acid vapours. Initially, the aerogels exhibited a light purple hue, which shifted to varying shades of green upon exposure to ammonia vapor. The most significant colour change occurred during the first exposure, indicating a strong interaction between the aerogel and the vapor. Conversely, exposure to acidic vapor caused the colour to darken to green, completing the cycle of reversible colour transitions.

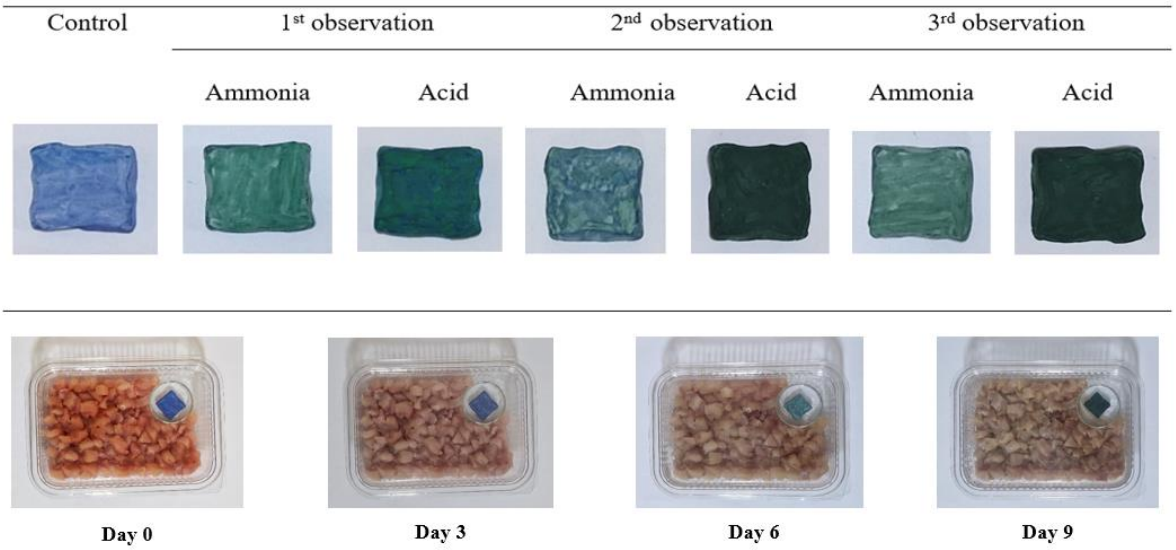

Fig. 6.13. (A) Reversibility of the BPF-based aerogels to ammonia and acetic acid vapours and (B) Apparent colour change of BPF-based aerogel in minced meat during storage at 4°C.

This cycle was repeated a second time with similar but slightly diminished responses. By the third exposure, however, the colour change became non-reversible. This irreversibility is attributed to the reduced porosity of the aerogel network, which trapped ammonia vapor within its structure, preventing its release. The diminished porosity likely resulted from structural changes induced by repeated vapor interactions, limiting the aerogel's ability to revert to its original state (Sohrabi et al., 2024). This highlights the aerogel's sensitivity to environmental changes and its potential limitations for extended applications.

6.3.4. Meat freshness monitoring

Microbial growth during meat spoilage is closely linked to the breakdown of protein compounds, releasing nitrogen-based volatile compounds (He et al., 2022). To monitor spoilage in minced meat, parameters including Total Viable Counts (TVC), pH, Total

Volatile Basic Nitrogen (TVB-N), and colour changes in bioactive aerogels were evaluated over storage days 0, 3, 6, and 9. As shown in **Table 6.4**, the initial TVC was 3.47 log CFU/g on day 0, and there was a progressive increase in TVC, TVB-N, and pH observed over time. Critical thresholds for meat spoilage, 15-25 mg/100 g for TVB-N and 10^7 CFU/g for TVC, are widely recognized, though some variations exist among countries (Tometri et al., 2020).

The bioactive aerogels aimed to monitor spoilage through visible colour changes rather than traditional microbial or chemical analyses. During storage, L* and a* values decreased, while b* and ΔE increased, reflecting colour changes in the aerogels. On days 0 and 3, the aerogels appeared navy blue, transitioning to green by day 6 (**Fig. 6.13**). As spoilage advanced and TVB-N exceeded acceptable limits, the aerogels turned dark green.

Table 6.4. Colour change of indicator and TVB-N (mg/100 g of meat), pH changes and TVC (log_{10}CFU/g) in minced meat during storage.

Parameters	**Time (Days)**			
	0	3	6	9
ΔE	-	14.7 ± 3.2^{c}	21.45 ± 2.1^{b}	34.49 ± 1.8^{a}
pH	5 ± 0.2^{d}	5.95 ± 0.4^{c}	9 ± 0.1^{b}	10.87 ± 0.1^{a}
TVB-N	12.3 ± 0.7^{d}	15.6 ± 0.4^{c}	23.5 ± 1.2^{b}	31.8 ± 0.9^{a}
TVC	3.47 ± 0.0^{c}	4.62 ± 0.2^{c}	6.36 ± 0.0^{b}	8.12 ± 0.1^{a}

*Values with different letters in each row are significantly different ($p < 0.05$); TVB-N: Total volatile bases - nitrogen; TVC: Total viable count

In a related study, Sobhan et al. (2022) used cellulose nanofiber film, methyl red, and poly-lactic acid indicators to monitor beef spoilage. Their indicators reported a ΔE of 20.45 on day 3, higher than the ΔE of 14.7 observed in this study. This discrepancy can be attributed to differences in storage temperature (23°C vs. refrigeration) and the type of meat analysed. Lower temperatures in the current study slowed spoilage and reduced ΔE changes in the indicator.

Based on spoilage limits, day 6 marked the onset of spoilage for minced meat. The bioactive aerogels successfully distinguished fresh meat from meat in early and advanced spoilage stages. Similarly, Dirpan et al. (2022) reported that spoilage in packaged beef occurred on day 6 under refrigeration. Unlike their findings, where microbial spoilage preceded TVB-N exceedance, this study observed microbial spoilage coinciding with the TVB-N threshold being breached. Notably, the bioactive aerogels exhibited a clear and timely colour change, confirming their potential as effective spoilage indicators for refrigerated chicken.

6.4. Conclusion

The study revealed that pure polyvinyl alcohol (PVA) aerogels display a denser, less porous structure, whereas incorporating cellulose fibers (CF) and nanocellulose (NC) creates a more organized, three-dimensional network. Adding butterfly Pea Flower Extract (BPFE) has minimal impact on the aerogel's internal morphology. FT-IR analysis confirms BPFE incorporation in the aerogel matrix, identified by characteristic bands associated with hydroxyl groups, alkanes, carboxylic acids, and other functional groups from both BPFE and the bioactive aerogels. The reduced relative crystallinity in PVA+CF+NC+BPFE aerogels, compared to PVA+CF+NC, is likely due to BPFE's low crystallinity, which may disrupt the crystallization of the PVA matrix when combined with the fillers. BPFE's phenolic compounds, inherently thermally unstable, contribute to a lower thermal breakdown temperature, although the aerogel matrix may offer some protection below 200°C.

Water absorption for aerogels with CF and CF/NC was 1116.99% and 1821.66%, respectively, while pure PVA aerogels had the lowest absorption at 460.66%. Adding CF and NC reduced density to below 0.1 g/cm^3 and increased porosity to over 90%. However, the antioxidant activity of the aerogels declined due to the dilution effect from CF and NC. High antioxidant capacity and progressive compound release were seen in hydrophobic and hydrophilic food simulant medium when aerogels from CF and NC were combined with the bioactive compound (i.e. BPFE). For hydrophobic foods, aerogel made of CF is more effective, but for hydrophilic foods, aerogel made of CF+NC is more promising. Along with providing quantitative and qualitative data for studies on cellulosic materials

derived from organic sources, the current study can be useful in active packaging and food preservation sectors.

Additionally, the colour-responsive properties of BPFE-based aerogels were also explored for food packaging applications. When anthocyanins concentration was set at 0.44 mg/100 mL, optimal colour shifts were observed in response to acidic and alkaline vapours. BPFE-based aerogels showed promise in detecting spoilage in minced chicken through visible colour changes corresponding to increased microbial load, pH, and total volatile basic nitrogen (TVB-N) levels.